ELSEVIER

International Journal of Pressure Vessels and Piping 75 (1998) 357–373

INTERNATIONAL JOURNAL OF
Pressure Vessels and Piping

Crack-opening-area analyses for circumferential through-wall cracks in pipes—Part I: analytical models

S. Rahman[1,*], F.W. Brust[2], N. Ghadiali[2], G.M. Wilkowski[2]

[1]*Department of Mechanical Engineering, The University of Iowa, Iowa City, IA 52242, USA*
[2]*Battelle Memorial Institute, Columbus, OH 43201-2693, USA*

Received 31 May 1996; accepted 30 June 1997

Abstract

Leak-before-break (LBB) analyses for circumferentially cracked pipes are currently being conducted in the nuclear industry to justify elimination of pipe whip restraints and jet impingement shields which are present because of the expected dynamic effects from pipe rupture. The application of the LBB methodology requires calculation of leak rates. The leak rates depend on the crack-opening area of the through-wall crack in the pipe. In addition to LBB analyses which assume a hypothetical flaw size, there is also interest in the integrity of actual leaking cracks corresponding to current leakage detection requirements in NRC Regulatory Guide 1.45, or for assessing temporary repair of Class 2 and 3 pipes that have leaks, as are being evaluated in ASME Section XI. The objectives of this study were to review, evaluate, and refine current predictive models for performing crack-opening-area analyses of circumferentially cracked pipes. A three-phase effort was undertaken to accomplish this goal. It is described here in a series of three papers generated from this study. In this first paper (Part I — Analytical models), a comprehensive review is performed to determine the current state-of-the-art in predicting crack-opening displacements for circumferentially cracked pipes under pure bending, pure tension, and combined bending and tension loads. Henceforth, new and improved analytical models and some preliminary results are presented for cases where current methods are inadequate or there are no available methods. Also, based on this review, a number of appropriate predictive models are identified for a systematic evaluation of their accuracy. The results of their evaluations will be presented and examined in the forthcoming companion papers (Part II — Model validations [1] and Part III — Off-center cracks, restraint of bending, thickness transition, and weld residual stresses) [2].

1. Introduction

Leak-before-break (LBB) analyses for circumferentially cracked pipes are currently being conducted in the nuclear industry to justify elimination of design requirements to account for dynamic effects during pipe rupture. This allows elimination of hardware, such as pipe whip restraints and jet impingement shields, which can impede accessibility to pipes and increase radiation exposure during maintenance operation and in-service inspection. In an LBB analysis for nuclear piping systems, the following approach is employed. First, it is necessary to show that the pipe system is not susceptible to fatigue, stress–corrosion cracking, creep, or waterhammer. Second, as a worst-case assumption, it is assumed that a through-wall crack exists with a maximum credible flaw size, which can be detected under normal operating loads with some safety factor on the leak rate. It is then desired that this through-wall crack will remain stable at normal operating plus safe shutdown earthquake loads with additional safety factors on either the crack size or the seismic loads. Further details of LBB methods are described in NUREG/CR-1061 Volume 3 [3], and the Draft Standard Review Plan, Section 3.6.3 [4] of the US Nuclear Regulatory Commission (NRC).

The application of the LBB methodology requires determination of leak rates. In addition to LBB analyses which assume a hypothetical flaw size, there is also interest in the integrity of actual leaking cracks corresponding to current leakage detection requirements in NRC Regulatory Guide 1.45, for assessing LBB applications where some cracking may be possible, or for assessing temporary repair of Class 2 and 3 pipes that have leaks as are being evaluated in ASME Section XI. Generally, the leak-rate calculations are performed for one of the following two purposes:

1. Given a flaw size, pipe dimensions, material stress–strain properties, and loading, the fluid leak rate through the crack needs to be determined. The aim is to estimate whether the given flaw size would result in a reliably detectable leak rate.
2. Given a leak rate, the COA needs to be determined.

* Corresponding author.

0308-0161/98/$ - see front matter
PII: S0308-0161(97)00081-1

Then, knowing the COA, pipe dimensions, material properties, and loading, the aim is to estimate the flaw size, which could subsequently be used to determine the pipe's load-carrying capacity.

For either of the two purposes, accurate models are needed to predict COA for subsequent leak-rate evaluations. Besides the finite element method, there are a number of engineering (or estimation) methods which are available in the current literature to determine the crack-opening characteristics of a pipe with a circumferential crack. However, due to the lack of systematic studies involving combined experimental and analytical efforts, the accuracy of these methods for different pipe materials, crack geometries, and loading conditions have yet to be evaluated [5].

Traditionally, the developments of the COA models have been focussed on idealized conditions for analyzing cracked pipes. For example, it is generally assumed that a simple circumferential through-wall crack exists in the base metal or the weld metal of the pipe with the crack located in the center of the bending plane. The crack-opening-area is calculated when this pipe is subjected to remote loads that may include pure bending or pure tension (generally pressure induced) or combined bending and tension. In reality, the loading conditions, the pipe and crack geometries, and the boundary conditions can be more complicated. For example, the crack in a pipe may become off-centered due to random imperfections around the pipe circumference, or pressure-induced bending may be restrained if the crack is close to a nozzle, or the crack may be located at the thickness transition (e.g. girth-weld crack in a nozzle), or the pipe may have significant weld residual stresses in addition to remote bending loads, etc. Currently, there are no engineering methods or guidelines available to analyze pipes under these conditions. While some of these aspects are applicable to LBB analyses, other aspects are more applicable to evaluating flaw stability for a real rather than a hypothetical flaw [5].

2. Objectives of the study

The objectives of this study were to review, evaluate, and refine current analytical models for conducting crack-opening-area analyses of pipes with circumferential through-wall cracks. A three-phase effort was undertaken to accomplish this goal [5]. In Phase 1, an in-depth review was conducted to examine current models and subsequently develop new and improved models for predicting crack-opening-area of through-wall cracked pipes. In Phase 2, the adequacy of these analytical models was evaluated by direct comparisons with test data from full-scale pipe fracture experiments. The results from twenty-five full-scale pipe fracture experiments, conducted in the past Degraded Piping Program [6], the International Piping Integrity Research Group Program (IPIRG),[7] and the Short Cracks in Piping and Piping Welds Program [8], were used to verify the analytical models. Finally, in Phase 3, several practical aspects of crack-opening due to off-center cracks, restraint of pressure-induced bending, cracks in thickness transition regions, and weld residual stresses were investigated to evaluate their effects.

Three technical papers corresponding to each of the above three phases are generated from this research. They are: (1) Crack-opening-area analyses for circumferential through-wall cracks in pipes. Part I — Analytical models, (2) Crack-opening-area analyzes for circumferential through-wall cracks in pipes. Part II — Model validations, and (3) Crack-opening-area analyses for circumferential through-wall cracks in pipes. Part III — Off-center cracks, restraint of bending, thickness transition, and weld residual stresses. This is the first paper in the series. In this paper (Part I — Analytical models), a comprehensive review is performed to determine the current state-of-the art in predicting crack-opening displacements for circumferentially cracked pipes under pure bending, pure tension, and combined bending and tension loads. Henceforth, new and improved analytical models and their preliminary results are presented for cases where current methods are inadequate or there are no available methods. Based on this review, a number of appropriate predictive models are identified for a systematic evaluation of their accuracy. Details of subject matters associated with the Phases 2 and 3 will be presented in the forthcoming companion papers [1,2].

3. Analytical models

For the prediction of crack-opening in a through-wall-cracked (TWC) pipe, it is desirable to have a mathematical model which is sufficiently accurate, relatively simple, and inexpensive to use. For example, a detailed finite element analysis, while generally accurate, would have very limited use because it would be expensive and time-consuming to be used routinely. What is needed is a relatively simple equation, or a set of equations, to estimate the crack-opening area (COA).

Simple mathematical models, often referred to as estimation models, are almost invariably based on assumptions necessary to minimize the need for elaborate numerical analyses. Typically, such assumptions lead to simpler representations of the material's stress–strain behavior, flaw shape and orientation, loading, and the boundary conditions [5]. Nevertheless, fracture mechanics models are required to evaluate the fracture response and crack-opening of a through-wall-cracked pipe. The available models can be broadly classified as:

- The linear-elastic fracture mechanics (LEFM)models; and
- The elastic–plastic fracture mechanics (EPFM)models.

This section provides a short summary of these models to

predict the crack-opening displacement (COD) in a through-wall-cracked pipe with particular emphasis on the EPFM models. Improvements and refinement of some of the models made in this study are also discussed. The companion paper (Part II — Model validations) will show how well these models perform by making direct comparisons with the experimental pipe fracture data [1].

3.1. Linear-elastic fracture mechanics models

The linear-elastic fracture mechanics models are based on the assumption that even at the maximum applied loads of interest, the material behavior everywhere in a pipe containing a through-wall crack remains linear-elastic. A number of linear-elastic solutions for through-wall cracks in pipes are available in the current literature. For examples, see the work done by Erdogan [9], Erdogan and Delale [10], Sanders [11,12], and Yoo and Pan [13]. Many of these elastic solutions in the literature appear in terms of the stress intensity factor (SIF) rather than the COD or COA. However, the available SIF solutions can be utilized to determine COD and COA using Castigliano's theorem, as described in Ref. [14] or, alternatively, in the work of Wuthrich [15].

The well-known GE/EPRI method [16–18] also permits the elastic calculation of COD for a through-wall-cracked pipe under various loading conditions. However, the main purpose of this method is for use as an elastic-plastic fracture-mechanics method. Further details of this method in the complete range between elastic and elastic–plastic conditions are described in a latter section of this paper.

Neglecting the crack-tip plasticity in LEFM models may lead to underestimates of COA for a given load acting on the pipe. Alternatively, for a prescribed remote displacement or rotation, an LEFM model will tend to overestimate the COA. In many practical situations, where the flaw size is small compared with the pipe circumference and where the loads are low, the error (positive or negative) caused by neglecting crack-tip plasticity should be insignificantly small.

3.2. Elastic–plastic fracture mechanics models

There are two basic types of elastic–plastic fracture mechanics methods used for predicting COD in a circumferential TWC pipe. They are:

- Finite element or numerical methods; and
- Engineering approximation (estimation) methods.

A finite element analysis can always be performed to determine the crack-opening displacements and precise crack-opening area for a given pipe geometry and material. However, for most practical applications of leak-before-break (LBB), a full finite element computation is not always needed. Also, such computations are too time-consuming and expensive to be used for routine LBB evaluations. Rather, compilations of finite element solutions for specific pipe and crack geometries and material constants, for instance from the GE/EPRI handbook, are typically used for crack-opening and fracture assessments [16–18]. The solutions available in the GE/EPRI handbook method [16] were improved in the NRC's Short Cracks in Piping and Piping Welds Program [8].

The estimation methods for predicting the fracture response and corresponding COD for TWC pipe involve either incorporating a plastic-zone correction into an elastic solution or approximating the crack compliance reduction via a reduced section analogy. The plastic-zone correction methods are the Paris/Tada method [19] and the LBB.NRC method [20]. A method based on the reduced thickness analogy is called the LBB.ENG2 method [21–23], and is discussed in this paper. Finally, a modification to the LBB.ENG2 method for predicting the J-integral and COD in a welded pipe, known as the LBB.ENG3 method [24–26]. is also developed in this study.

3.2.1. Idealization of material properties

In general, the fracture response and COA predictions by the estimation models require an analytic description of the material properties. For example, it is generally assumed that the constitutive law characterizing the material's stress–strain response can be represented by the well-known Ramberg–Osgood model

$$\frac{\epsilon}{\epsilon_0} = \frac{\sigma}{\sigma_0} + \alpha\left(\frac{\sigma}{\sigma_0}\right)^n \tag{1}$$

in which σ_0 is a reference stress usually assumed to be the yield stress, $\epsilon_0 = \sigma_0/E$ is the associated reference strain, E is the modulus of elasticity, and α and n are strain-hardening parameters usually chosen from a best fit of laboratory data. This representation of the stress–strain curve is necessary, since the J-integral and COD in most estimation schemes are formulated based on a power-law idealization.

In characterizing the fracture toughness of the materials, the ASTM J-resistance curve (J-R curve) is typically used. The J–R curve, which is usually generated from small specimens cut from the pipe (e.g. the compact tension [$C(T)$] specimen), can be conveniently modeled by a power-law equation of the form

$$J_R(\Delta a) = J_{Ic} + C\left(\frac{\Delta a}{r}\right)^m \tag{2}$$

in which Δa is the crack length extension during crack growth, J_{Ic} is the fracture toughness at crack initiation, and C and m are the power-law parameters from a best fit of the experimental data. In Eq. (2), r is a convenient normalizing parameter with a value of unity and the same units as Δa. For example, if J and Δa are expressed in kJ/m^2 and mm, the dimension of C also becomes kJ/m^2 if $r = 1$ mm. Because the C(T) specimens are small, large extrapolation

of the data is often required in order to predict crack growth in a pipe, particularly for the large diameter pipes. Note that 'Δa' here is the physical crack extension, i.e. without blunting. This is because blunting is automatically accounted for in the finite element method as well as in the pipe estimation schemes.

3.2.2. Crack-opening-area analysis for J-controlled crack growth

In order to evaluate crack-opening displacements for a growing crack, the criteria for crack growth must be specified. Recent analytical, experimental, and computational studies on this subject indicate that the energy release rate, also known as the J-integral [27,28], is the most viable fracture parameter for characterizing crack initiation, stable crack growth, and subsequent instability in ductile materials. This suggests that J can be conveniently used to assess structural integrity for both leak-before-break and in-service flaw acceptance criteria in degraded piping systems. It is, however, noted that the parameter J still possesses some theoretical limitations. For example, the Hutchinson–Rice–Rosengren (HRR) singular field [27–29] may not be valid in the case of certain amounts of crack extension where J ceases to act as an amplifier for this singular field. Nevertheless, the possible error is considered tolerable if the relative amount of crack extension stays within a certain limit, and if elastic unloading and non-proportional plastic loading zones around a crack tip are surrounded by a much larger zone of nearly proportional loading controlled by the HRR field [30]. Under this condition of J-dominance, both the onset and limited amount of crack growth can be correlated to the critical values of J and J-resistance curve, respectively [31].

The applications of the J-integral in describing crack-driving force, crack growth, and subsequent crack-opening in a pipe are well-established for pure bending or pure tension loads [16–26]. Discussions on the conditions for achieving J-dominance and the suitability of J as a fracture parameter for combined bending and tensile loadings have been presented by Shih [32] and Shih and Hutchinson[33] by studying the single-edge notch specimen. Additional studies based on finite element analysis of the single-edge notch specimen subjected to combined tension and bending have recently appeared [34,35]. An important result obtained by Sonnerlind and Kaiser [35] indicates that the value of J is essentially independent of whether tension is applied followed by bending, bending then tension or both tension and bending are applied proportionally. This is not intuitively obvious since such loading clearly violates the hypothesis (necessary for the valid J-tearing theory) of proportional loading. Further discussions on the validity of J for combined bending and tension are available in Ref. [36]. Details of finite element analyses for combined loads and the results produced by the incremental and deformation plasticity theories are given in a separate study by the authors [37].

4. Estimation models for EPFM analysis

Consider a simple through-wall-cracked pipe with mean radius, R_m, wall thickness, t, and a crack angle, 2θ, located in the center of the bending plane. Several loading conditions can be considered. For example, the pipe may be under a pure bending moment, M, or pure tension (axial), P, due to internal pipe pressure, p, or combined bending (M) and tension (P). Fig. 1 shows a schematic representation of a through-wall-cracked pipe subjected to combined bending and tension. In a typical estimation scheme, it is generally assumed that the load-point rotation and axial displacement (or stretch) due to the presence of a crack, ϕ^c and Δ^c, the relevant crack-driving force, J, and center-crack-opening displacement, δ, allow additive decomposition into elastic and plastic components given by

$$\phi^c = \phi^c_e + \phi^c_p \tag{3}$$

$$\Delta^c = \Delta^c_e + \Delta^c_p \tag{4}$$

$$J = J_e + J_p \tag{5}$$

$$\delta = \delta_e + \delta_p \tag{6}$$

where the subscripts 'e' and 'p' refer to the elastic and plastic contributions, respectively. In the elastic range, ϕ^c_e and M, and Δ^c_e and P are uniquely related. In addition, if the deformation theory of plasticity holds, a unique relationship also exists between ϕ^c_p and M, and Δ^c_p and P. These relationships provide important information in determining J or COD in a pipe [16–26].

In this paper, several estimation methods currently

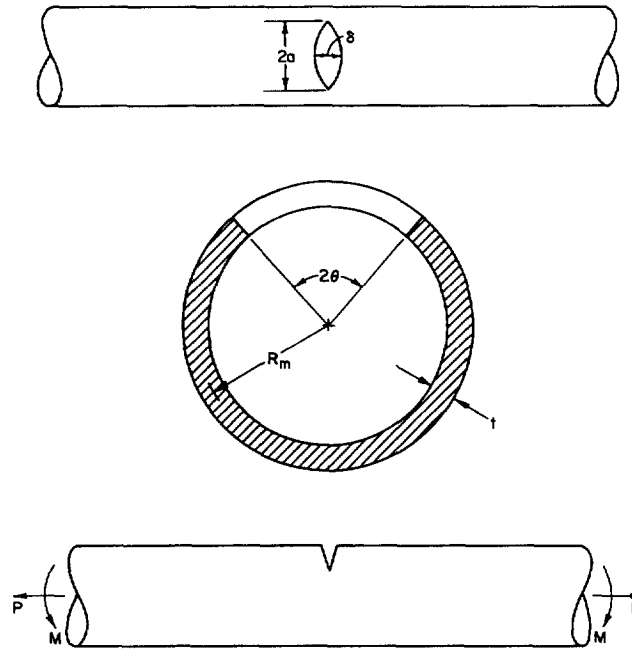

Fig. 1. Schematic representation of pipe with a circumferential through-wall crack subjected to bending and tension.

available in the literature are reviewed for predicting fracture response and crack-opening displacements of a circumferential TWC pipe under various loads. The five different estimation methods considered were:

- The GE/EPRI method;[16–18]
- the Paris/Tada method;[19]
- the LBB.NRC method;[20]
- the LBB.ENG2 method;[21–23] and
- the LBB.ENG3 method.[24–26]

In the following paragraphs, a short summary for each of these estimation schemes is provided with the estimation formulas for both J-integral and COD. The evaluations of COD are discussed for various loading conditions, e.g. pure bending, pure tension, and combined bending and tension. For brevity, the J-integral evaluations are discussed only for pure bending.

4.1. The GE/EPRI method

4.1.1. J-integral

The GE/EPRI method is based on a compilation of finite element solutions for TWC pipes using the deformation theory of plasticity. These solutions are catalogued in Refs [16–18] for various geometric and material parameters. For pure bending in pipes containing a through-wall crack, the J-integral is calculated by Eq. (5) in which the elastic component J_e, and the plastic component J_p, are given by [16,17]

$$J_e = \pi a\left(\frac{R_m}{I}\right)^2 F^2(a/b, R_m/t)\frac{M^2}{E} \tag{7}$$

$$J_p = \alpha\sigma_0\epsilon_0 c\frac{a}{b}h_1^B(a/b, n, R_m/t)\left(\frac{M}{M_0}\right)^{n+1} \tag{8}$$

where $a = R_m\theta$ is half of the crack length at the mean diameter, $b = \pi R_m$ is half of the mean pipe circumference, $c = R_m(\pi - \theta)$ is half of the uncracked ligament of the pipe, $I \simeq \pi R_m^3 t$ is the moment of inertia of an uncracked pipe cross-section about its centroidal axis, $F(\theta/\pi, R_m/t)$ and $h_1^B(a/b, n, R_m/t)$ are the elastic and plastic influence functions, respectively, for the J-integral under pure bending that are tabulated in Ref. [17], and

$$M_0 = 4\sigma_0 R_m^2 t\left[\cos\frac{\theta}{2} - \frac{1}{2}\sin\theta\right] \tag{9}$$

is a reference moment representing the limit moment for a TWC pipe also under pure bending if σ_0 is the collapse stress. Similar functional forms can be written for the tension case and the combined bending and tension case with the corresponding influence functions compiled in the pertinent references.

4.1.2. Center-crack-opening displacement

The following are the elastic and plastic solutions for the center-crack-opening displacement of a pipe under various loading conditions:

Bending. The elastic and plastic parts of the center-crack-opening displacement for the case of pure bending, as defined by the GE/EPRI method, are [16–18]

$$\delta_e = 4a\frac{R_m}{I}V_1^B(a/b, R_m/t)\frac{M}{E} \tag{10}$$

$$\delta_p = \alpha\epsilon_0 a h_2^B(a/b, n, R_m/t)\left(\frac{M}{M_0}\right)^n \tag{11}$$

where $V_1^B(a/b, R_m/t)$ and $h_2^B(a/b, n, R_m/t)$ are the elastic and plastic influence functions, respectively, for COD under pure bending.

Tension. The GE/EPRI influence functions for the case of a pure tension load, P, were compiled using a tensile load caused by the end-capped pipe with internal pressure, p, applied at the ends of the pipe. The corresponding equations for the elastic and plastic CODs are [16–18]

$$\delta_e = \frac{2a}{\pi R_m t}V_1^T(a/b, R_m/t)\frac{P}{E} \tag{12}$$

$$\delta_p = \alpha\epsilon_0 a h_2^T(a/b, n, R_m/t)\left(\frac{P}{P_0}\right)^n \tag{13}$$

where $V_1^T(a/b, R_m/t)$ and $h_2^T(a/b, n, R_m/t)$ are the elastic and plastic influence functions, respectively, for crack-opening displacement under pure tension, P is the axial tensile force due to an internal pipe pressure, and

$$P_0 = 2\sigma_0 R_m t\left[\pi - \theta - 2\sin^{-1}\left(\frac{1}{2}\sin\theta\right)\right] \tag{14}$$

is a reference load representing the limit load of a TWC pipe under pure tension if σ_0 is the collapse stress.

Combined Bending and Tension. For a pipe subjected to a combined bending and tension loading, the elastic and plastic CODs are [16–18]

$$\delta_e = 4a\frac{R_m}{I}V_1^B(a/b, R_m/t)\frac{M}{E} + \frac{2a}{\pi R_m t}V_1^T(a/b, R_m/t)\frac{P}{E} \tag{15}$$

$$\delta_p = \alpha\epsilon_0 a h_2^{B+T}(a/b, n, R_m/t, \lambda)\left(\frac{P}{P_0'}\right)^n \tag{16}$$

where $h_2^{B+T}(a/b, n, R_m/t, \lambda)$ is the plastic influence function for crack-opening displacement under combined bending and tension,

$$P_0' = \frac{1}{2}\left[-\frac{\lambda P_0^2 R_m}{M_0} + \sqrt{\left(\frac{\lambda P_0^2 R_m}{M_0}\right)^2 + 4P_0^2}\right] \tag{17}$$

is another reference load representing the limit load of a TWC pipe under combined bending and tension if σ_0 is the collapse stress, and $\lambda = M/PR_m$ is the load factor.

The values of the above influence functions for TWC pipes under pure bending, pure tension, and combined bending and tension were compiled by Kumar et al. [16,17]

and Kishida and Zahoor [18] for specific pipe geometries (e.g. $R_m/t = 5$, 10, and 20), crack sizes ($a/b = 1/16$, 1/8, 1/4, and 1/2), and material constants ($n = 1, 2, 3, 5, 7$). For a pipe with an arbitrary geometry and material properties, the corresponding influence functions can be evaluated from multiple interpolation of these functions at the predetermined values of R_m/t, a/b (i.e. θ/π), n, and λ. See Refs [16–18] for further details on these functions.

As an alternative, these plastic influence functions can also be evaluated for a fixed internal pressure and an increasing bending moment using procedures similar to those used for tension or bending alone. For example, the calculated influence functions can be determined for an internal pressure of 15.51 MPa (2250 psi) and 7.24 MPa (1050 psi) simulating operating conditions at PWR and BWR plants, respectively. Accordingly, the plastic COD is

$$\delta_p = \alpha\epsilon_0 a h_2^T(a/b, n, R_m/t)\left(\frac{P}{P_0}\right)^n + \alpha\epsilon_0 a h_2^{B+T}(a/b, n, R_m/t)\left(\frac{M}{M_0}\right)^n \quad (18)$$

where $h_2^T(a/b, n, R_m/t)$ is plastic influence function for COD under pure tension, and $h_2^{B+T}(a/b,n,R_m/t)$ is plastic influence function for COD under bending in presence of a fixed tension load. The first term in the right hand side of Eq. (18) represents the plastic contribution of COD under tensile load before the application of bending moment. By no means, Eq. (18) represents linear superposition, since h_2^{B+T} function always includes the effects of tension under combined bending and tension loads. Similar equations can also be derived for J and other fracture parameters of interest.

4.1.3. Plastic-zone size correction in the GE/EPRI method

In Ref. [38], it has been claimed that the linear-elastic solutions of J, COD, and other fracture parameters of interest underestimate the actual values when M/M_0 exceeds 0.5 and the plastic components of the above parameters are too small, e.g. for large n values. This is the apparent reason why Kumar et al. [17] extended the plastic-zone size formula established by Rice [27] for the antiplane shear problem. According to Ref. [17], the effective crack length (half), a_e, is given by

$$a_e = a + \kappa r_y \quad (19)$$

where

$$r_y = \frac{1}{\beta_1\pi}\frac{n-1}{n+1}\left(\frac{K_I}{\sigma_0}\right)^2 \quad (20)$$

K_I is the mode-I stress intensity factor, and

$$\kappa = \begin{cases} \dfrac{1}{1+(M/M_0)^2} & \text{(pure bending)} \\ \dfrac{1}{1+(P/P_0)^2} & \text{(pure tension)} \end{cases} \quad (21)$$

The value of β_1 in Eq. (20) depends on the state of stress, e.g. $\beta_1 = 2$ for plane stress and $\beta_1 = 6$ for plane strain. For a through-wall-cracked pipe under pure bending or tension, the stress state is dominated by the plane stress condition (i.e. $\beta_1 = 2$).

Eq. (19) was developed in order to increase the value of elastic J or COD when the applied load becomes closer to the reference load, e.g. when M becomes closer to M_0. There is no sound technical justification for the choice of the $1/[1 + (M/M_0)^2]$ or $1/[1 + (P/P_0)^2]$ function in Eq. (21) except ensuring the continuity of the partial derivatives of J with respect to applied load at $M = M_0$ or $P = P_0$. Past experience by the authors suggests that when using the GE/EPRI method for TWC pipes, the plastic-zone correction in the elastic solution may be a contributor to the overprediction of applied crack-driving force. Nevertheless, it has been suggested in Refs [16–18] to use the plastic-zone correction in the elastic solution, i.e.

$$J_e(a, M) = J_e(a_e, M) \quad (22)$$

$$\delta_e(a, M) = \delta_e(a_e, M) \quad (23)$$

for a pipe under pure bending. Similar plastic-zone corrections can also be used for a pipe subjected to pure tension or combined bending and tension.

4.2. The Paris/Tada method

4.2.1. J-integral

In the Paris/Tada method [19], J is obtained using an interpolation between the linear-elastic and fully-plastic limit-load solutions. In effect, the procedure uses the techniques developed in Refs [39,40] for a planar fracture specimen appropriately adapted for a through-wall-cracked pipe. Thus, J calculated by this method depends only on the cracked-pipe geometry and flow stress, and does not explicitly account for hardening behavior of the material.

For linear-elastic and rigid-plastic conditions in through-wall-cracked pipes, the moment-rotation and J-rotation relations are well-established [19]. The Paris/Tada method interpolates between these two solutions by artificially increasing the crack size using a plastic-zone size correction and substituting this artificially increased crack size into the elastic solution to obtain the moment-rotation relation in the elastic–plastic regime. This procedure is based on the Irwin estimate [41] of the size of the plastic zone that is given by

$$\theta_e = \theta + \frac{1}{\beta_1\pi R_m}\left(\frac{K_I}{\sigma_y}\right)^2 \quad (24)$$

where θ_e is the effective crack angle (half), σ_y is the yield strength of the material, and $\beta_1 = 2$ or 6 depending on whether plane stress or plane strain conditions apply, respectively. The estimate of the plastic-zone size in Eq. (24) is only accurate for small plastic zones. Because Paris/Tada attempts to estimate J throughout the entire range between elastic and rigid plastic response, a method

was developed to interpolate between elastic and fully plastic conditions. This interpolation method amounts to modifying β_1 in Eq. (24). Then, β_1 is not 2 or 6, but rather is determined in a somewhat complicated fashion which depends on the current load, as detailed in Ref. [19].

From linear-elastic fracture mechanics, it can be shown that the moment and the elastic rotation are related via [19–21,24–26]

$$M = \frac{E\pi R_m^2 t}{I_B(\theta)}\phi_e^c \tag{25}$$

where $I_B(\theta)$ is a bending compliance function defined in Ref. [19]. Using the effective crack size, θ_e (i.e. applying a plastic-zone correction) and total rotation, ϕ^c in place of θ and ϕ_e^c in Eq. (25) and the expression for a rigid-plastic moment, the final equations for J_e and J_p by the Paris/Tada method for the case of pure bending are [19]

$$J_e = \frac{K_I^2}{E} \tag{26}$$

$$J_p = \frac{\sigma_y R_m[\sin(\theta/2) + \cos\theta]}{M_{RP}(\theta)} \int_0^{\phi_p^c} M(\theta)\mathrm{d}\phi_p^c \tag{27}$$

where

$$K_I = \frac{M}{\pi R_m^2 t} F_B(\theta)\sqrt{\pi R_m \theta} \tag{28}$$

is the stress intensity factor for a TWC pipe under pure bending with $F_B(\theta)$ representing the appropriate geometry function and M_{RP} is the rigid-plastic moment from limit-load analysis given by

$$M_{RP} = 4\sigma_f R_m^2 t\left[\cos\frac{\theta}{2} - \frac{1}{2}\sin\theta\right] \tag{29}$$

where σ_f is the flow stress of the material. Explicit functional forms of $F_B(\theta)$ and $I_B(\theta)$ are given in Ref.[19].

4.2.2. Center-crack-opening displacement

According to Ref.[19], the elastic crack-opening area, A_{ce}, for a TWC pipe under combined bending and tension can be derived from the energy method (Castigliano's theorem) which gives

$$A_{ce} = \frac{\pi R_m^2}{E}[\sigma_B I_B(\theta) + \sigma_T I_T(\theta)] \tag{30}$$

where $I_T(\theta)$ is the tensile compliance function defined in Ref.[19], $\sigma_B = M/(\pi R_m^2 t)$ is the nominal bending stress at the mean pipe diameter, and $\sigma_T = P/2\pi R_m t$ is the nominal tensile (axial) stress for an uncracked pipe section. Further simplification of Eq. (30), details of which are given in Ref.[19], yields

$$A_{ce} \simeq \frac{\pi R_m^2}{E} I_T(\theta)\left[\sigma_B \frac{3+\cos\theta}{4} + \sigma_T\right] \tag{31}$$

Eqs. (30) and (31) are valid only for the linear-elastic condition. However, for the elastic–plastic condition, Paris and Tada extended these equations by incorporating plastic-zone corrections discussed previously. Accordingly, for an EPFM analysis, the crack-opening area is given by

$$A_c \simeq \frac{\pi R_m^2}{E} I_T(\theta_e)\left[\sigma_B \frac{3+\cos\theta_e}{4} + \sigma_T\right] \tag{32}$$

where θ_e is half of the effective crack angle already defined in Eq. (24). Assuming an elliptical crack-opening shape, the total center-crack-opening displacement is

$$\delta \simeq \frac{2R_m^2}{aE} I_T(\theta_e)\left[\sigma_B \frac{3+\cos\theta_e}{4} + \sigma_T\right] \tag{33}$$

Setting $\sigma_T = 0$ or $\sigma_B = 0$ in Eq. (33), one can compute the COD under pure bending or pure tension, respectively.

4.3. The LBB.NRC method

4.3.1. J-integral

The LBB.NRC method[20] for TWC pipes subjected to bending is similar to the Paris/Tada method described earlier. However, the elastic geometry function, $F_B(\theta)$, was derived independently based on Sanders' elastic solutions [11,12]. The plastic component of rotation due to a crack is written as

$$\phi_p^c = \alpha\left(\frac{\sigma}{\sigma_f}\right)^{n-1}\phi_e^c \tag{34}$$

with $\phi_e^c = \phi_e^c(\theta_e)$ from the Paris/Tada solution. Hence, the elastic component of rotation is increased by an interpolation type of Irwin plastic-zone correction and the plastic component of rotation is increased or decreased depending on the current applied stress level. In the LBB.NRC method, the effects of strain-hardening are incorporated in the evaluation of the J-integral.

4.3.2. Center-crack-opening displacement

The crack-opening area calculations by the LBB.NRC method are almost identical to those by the Paris/Tada method discussed earlier. According to Ref. [20], Eq. (32) and Eq. (33) are also used to compute COA and COD, respectively. However, in these equations, the effective crack angle, θ_e is not the same as in the Paris/Tada method. The β_1 term in the equation for plastic-zone correction (see Eq. (24)) in the Paris/Tada and the LBB.NRC method is calculated by forcing the solution to reach the limit load of a cracked pipe for large values of the stress intensity factor. Further details on the derivation of β_1 are available in Refs [19,20].

4.4. The LBB.ENG2 method

4.4.1. J-integral

The LBB.ENG2 method was originally developed by Brust [21] to compute the energy release rate and crack-opening

for through-wall-cracked pipes. It involves an equivalence criterion incorporating a reduced thickness analogy for simulating system compliance due to the presence of a crack in a pipe. Detailed derivations of both elastic and plastic components of the J-integral in this method are available in Refs [21–23]. Only the final expressions are presented here.

For a pipe under pure bending, the elastic component of J, J_e, by the LBB.ENG2 method is identical to that by the Paris/Tada method and hence, is given by Eq. (26). However, the equation for the geometry function, $F_B(\theta)$, was obtained from the LBB.NRC method. The plastic component of J, J_p, was calculated by invoking the energy interpretation of J and hence, by integrating the moment-rotation ($M-\phi_p^c$) curve. The $M-\phi_p^c$ relation was derived from the solution of the ordinary differential equations for a beam representing an uncracked pipe with a reduced thickness (stiffness) and power-law constitutive properties. The reduced (equivalent) thickness was approximated by forcing the limit moment of this uncracked pipe to be equal to that of the actual cracked pipe. Finally, the plastic component of J, J_p, is given by [21,23]

$$J_p = \frac{\alpha}{E\sigma_0^{n-1}} \frac{\pi R_m}{2(n+1)} H_B(n,\theta) L_B(n,\theta) I_B(\theta) \left(\frac{M}{\pi R_m^2 t}\right)^{n+1} \tag{35}$$

where

$$H_B(n,\theta) = \frac{4\theta F_B(\theta)^2}{I_B(\theta)} + \frac{1}{L_B(n,\theta)} \frac{\partial L_B(n,\theta)}{\partial \theta} \tag{36}$$

$$L_B(n,\theta) = \left[\frac{\pi}{4\left\{\cos\left(\frac{\theta}{2}\right) - \frac{1}{2}\sin\theta\right\}}\right]^{n-1} \left(\frac{\pi}{4\hat{K}}\right)^n \tag{37}$$

with

$$I_B(\theta) = 4\int_0^\theta \theta F_B(\theta)^2 d\theta \tag{38}$$

$$\hat{K} = \frac{\sqrt{\pi}}{2} \frac{\Gamma\left(1+\frac{1}{2}n\right)}{\Gamma\left(\frac{3}{2}+\frac{1}{2}n\right)} \tag{39}$$

and

$$\Gamma(u) = \int_0^\infty \zeta^{u-1}\exp(-\zeta)d\zeta \tag{40}$$

representing the gamma function. Further details on the simplified forms of these functions are available in Refs [21–23].

4.4.2. Center-crack-opening displacement

Bending. For the case of a pure bending load, the elastic COD solution is the same as in the GE/EPRI method (i.e. Eq. (10)). Initially, there were attempts to use some of the closed-form solutions, for instance, as developed in Ref. [13]. However, these analytical solutions were smaller by a factor of three compared with the numerical solutions as well as with the experimental data. Therefore, the numerical solutions of the GE/EPRI method were selected for the elastic component of COD in this method. The plastic component of COD is obtained from

$$\delta_p = R_m\left[1 + \sin\frac{\theta}{2}\right]\phi_p^c \tag{41}$$

where the plastic rotation in the presence of a crack, ϕ_p^c, is given by [21–23]

$$\phi_p^c = L_B(n,\theta)\frac{\alpha}{E\sigma_0^{n-1}}\frac{I_B(\theta)}{(\pi R_m^2 t)^n}M^n \tag{42}$$

The term $R_m[1 + \sin(\theta/2)]$ in Eq. (41) is the distance from the rigid-plastic neutral axis to the center of the crack.

Tension. For the pure tension load case, the estimate of δ has a functional form similar to that for the bending case. The crack-opening displacement is again separated into elastic and plastic components. The elastic COD is given by the same equation of the GE/EPRI method (i.e. Eq. (12)). The plastic COD is given by

$$\delta_p = \frac{\alpha\epsilon_0\left(\frac{\sigma_T}{\sigma_0}\right)^{n-1}}{1-\frac{\theta}{\pi}-\frac{2}{\pi}\sin^{-1}\left(\frac{1}{2}\sin\theta\right)} + R_m\left[1+\sin\frac{\theta}{2}\right]\phi_p^c \tag{43}$$

In Eq. (43), the first term is due to the tension load and the second term is due to the induced bending caused by the tension load on the cracked pipe. Note that ϕ_p^c in this equation is the plastic rotation in the presence of the crack that is caused only by the pressure or tension-induced bending. This bending moment can be inserted in Eq. (42) to obtain ϕ_p^c.

Combined bending and tension. For combined bending and tension, the elastic COD is obtained by superposing the solutions for pure bending and pure tension, which are given by Eq. (10) and Eq. (12), respectively. The plastic COD is given by the same form as shown by Eq. (43), but ϕ_p^c in that equation now includes both the applied moment and the induced bending due to tension.

4.5. The LBB.ENG3 method

4.5.1. J-integral

The LBB.ENG3 method, developed by Rahman and Brust [24–26], improves the computation of the J-integral and COD for TWCs in pipe welds by incorporating weld-metal strength properties. The method is similar to the LBB.ENG2 method and is also based on an equivalence

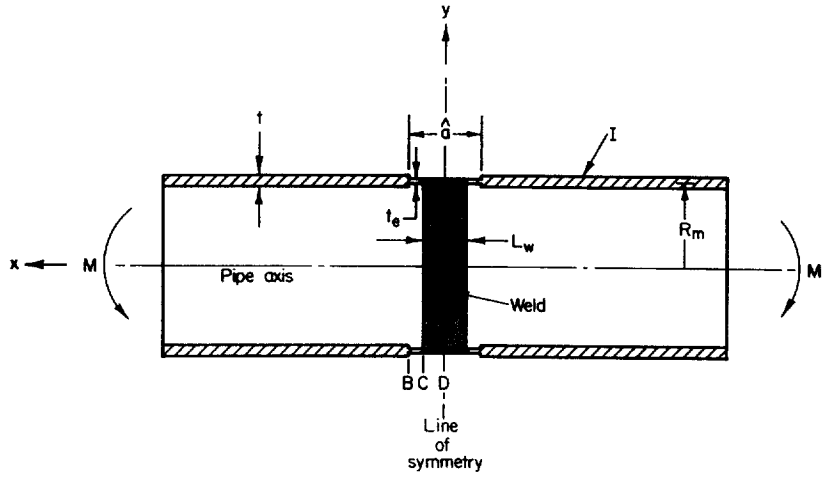

Fig. 2. Reduced section analogy in the LBB.ENG3 method.

criterion incorporating reduced thickness analogy for simulating system compliance due to the presence of a crack in the pipe. Fig. 2 shows a schematic for the reduced section analogy by the LBB.ENG3 method for analyzing welded pipes with a through-wall crack in the center of the weld.

The elastic solution obtained by this method is identical to that obtained by the LBB.ENG2 or the LBB.NRC method and is given by Eq. (26) (for pure bending) presented earlier. The plastic solution for the J-integral, also under pure bending, is

$$J_p = \frac{\alpha_1}{E_1\sigma_{01}^{n_1-1}}\frac{\pi R_m}{2(n_1+1)}H_B(n_1,n_2,\theta)L_B(n_1,n_2,\theta)I_B(\theta) \times \left(\frac{M}{\pi R_m^2 t}\right)^{n_1+1} \tag{44}$$

in which the additional subscripts '1' and '2' on the variables E, σ_0, α, and n are needed to represent base and weld metal properties, respectively. In Eq. (44), $H_B(n_1,n_2,\theta)$ and $L_B(n_1,n_2,\theta)$ are the algebraic functions defined by

$$H_B(n_1,n_2,\theta) = \frac{1}{I_B(\theta)}\frac{\partial I_B(\theta)}{\partial\theta} + \frac{1}{L_B(n_1,n_2,\theta)}\frac{\partial L_B(n_1,n_2,\theta)}{\partial\theta} \tag{45}$$

and

$$L_B(n_1,n_2,\theta) = \frac{\left(\frac{M}{M_{01}}\right)^{n_1}\left(\frac{\hat{a}}{2}-\frac{L_w}{2}\right)\left(\frac{t}{t_e}\right)^{n_1} + \left(\frac{M}{M_{02}}\right)^{n_2}\frac{L_w}{2}\left(\frac{t}{t_e}\right)^{n_2}}{\left(\frac{M}{M_1^*}\right)\epsilon_{01}\left(\frac{\hat{a}}{2}-\frac{L_w}{2}\right)\frac{t}{t_e} + \left(\frac{M}{M_2^*}\right)\epsilon_{02}\frac{L_w}{2}\frac{t}{t_e}} \times \frac{1}{\alpha_1\left(\frac{M}{M_1^*}\right)^{n_1-1}} \tag{46}$$

respectively, where for material i ($i=1$ for base metal, $i=2$ for weld metal), σ_{0i} is the reference stress, α_i and n_i are the Ramberg–Osgood parameters, $\epsilon_{0i} = \sigma_{0i}/E_i$ is the associated reference strain, L_w is the width of the weld in the pipe, $\hat{a}$ is the length of reduced thickness, t_e is the equivalent thickness of the pipe, $M_i^* = \sigma_{0i}I/R_m$ is the elastic bending moment corresponding to reference stress, σ_{0i}, and

$$M_{0i} = \frac{4K_iI\hat{K}_i}{\pi R_m} \tag{47}$$

with $K_i = \sigma_{0i}/(\alpha_i\epsilon_{0i})^{1/n_i}$ and

$$\hat{K}_i = \frac{\sqrt{\pi}}{2}\frac{\Gamma\left(1+\frac{1}{2}n_i\right)}{\Gamma\left(\frac{3}{2}+\frac{1}{2}n_i\right)} \tag{48}$$

Clearly, the $H_B(n_1,n_2,\theta)$ and $L_B(n_1,n_2,\theta)$ functions in Eq. (44) are more complex than their counterparts are in Eq. (35) due to the inclusion of both base and weld metal properties. See Refs [24–26] for fundamental details on the development of the LBB.ENG3 method.

4.5.2. Center-crack-opening displacement

The equations for the estimates of COD by the LBB.ENG3 method are identical to those of the LBB.ENG2 method, except the plastic rotation due to the presence of a crack is evaluated considering the tensile properties of both the base and weld metals. According to this method, ϕ_p^c can be obtained from

$$\phi_p^c = L_B(n_1,n_2,\theta)\frac{\alpha_1}{E_2\sigma_{01}^{n_1-1}}\frac{I_B(\theta)}{(\pi R_m^2 t)^{n_1}}M^{n_1} \tag{49}$$

Once again, further details can be found in Refs [24–26].

Note that Eq. (44) and Eq. (49) have characteristics similar to those of Eq. (35) and Eq. (42) required to calculate J_p and ϕ_p^c, respectively, for a base-metal crack (the LBB.ENG2 method). However, from Eq. (44) and Eq. (49), it can be seen that the tensile strength properties of both base and weld metals are accounted for in calculating the J-integral and plastic rotation. Eq. (44) and Eq. (49) are strongly dependent on the base metal properties, but the weld

metal properties are also considered via L_B and H_B-functions. When differences in the base metal and weld metal properties vanish, it can be shown that Eqs. (44) and (49) degenerate to Eq. (35) and Eq. (42), respectively, as one would expect. Hence, the LBB.ENG2 method can be treated as a special case of the more general LBB.ENG3 method.

4.6. Other methods

In addition to the estimation methods discussed above, there are a few other methods to estimate COA for TWC pipes. For example, Wuthrich [15] has given an expression for COA for through-wall axial and circumferential cracks in pipes subjected to membrane forces. The results are presented as the product of a plasticity correction factor, γ, and the area of crack opening, A_{ce}, calculated by linear-elastic analysis, that is,

$$A_c = \gamma A_{ce} \tag{50}$$

Wuthrich gives γ based on both Irwin [41] and Dugdale [42] plastic-zone corrections for small-scale yielding. A comparison of the two approaches, made in Ref. [43], suggests that for small values of σ/σ_y (σ is the nominal applied stress) the two approaches give approximately the same result. For larger values of σ/σ_y, the plasticity correction factors associated with the two approaches deviate from each other, but for larger σ/σ_y values the small-scale yielding condition is violated and neither approach should be expected to be accurate. Instead, it may be more appropriate to use another model based on the assumption that the uncracked ligament is fully yielded. One such model, proposed by Smith [44], gives the following expression for COA for a circumferential through-wall crack in a pipe under pure bending:

$$A_c = 4R_m^2\phi_p^c\left[1 - \cos\frac{\theta}{2} + \frac{1}{2}\sin\theta\right] \tag{51}$$

While both the linear-elastic and the small-scale yielding models are useful in specific situations, they cannot be expected to provide accurate COA estimates over the entire range of load magnitudes, flaw sizes, and material types of interest in nuclear piping systems. The main reason is that a large number of situations are such that the crack-tip plastic deformation can be characterized by neither linear elasticity nor small-scale yielding. Rather, the analysis problem is elastic–plastic, requiring nonlinear analysis methods. Specific examples showing comparisons with pipe test data are given in a companion paper [1].

In the above, the discussions are focussed on COD rather than COA. However, it is often required to calculate COA for leak-rate predictions. Typically, the COA is estimated by assuming various crack-opening shapes, which are: ellipse, rectangle, diamond. Out of these three crack-opening shapes, the elliptical shape has been used quite extensively for LBB evaluations [5–8]. Indeed, there are experimental data which show that the elliptical profile best represents the crack-opening shape for a stationary crack in a pipe [5–8]. Further details of crack-opening shape and its numerical evaluation by the finite element method are presented in the companion paper [1].

5. The newly generated influence functions

Earlier studies on fracture response and crack-opening in pipes were concerned for the most part with larger cracks (i.e. $\theta/\pi \geq 30\%$) where the nominal failure stresses were below yield. The estimation methods developed to date, some of which are described here, are well-suited for analyzing pipes with large cracks. The ability of these methods to predict crack-opening for small cracks ($\theta/\pi \leq 12\%$) has not been established even though such small cracks are often the concern in practical LBB analyses. A short crack is typical of one for LBB analyses in large diameter pipes. Indeed, the finite element solutions compiled in the GE/EPRI handbook [17] appear quite inadequate for small-size cracks. This paper presents new results from a series of finite element analyses and are tabulated in the spirit of the GE/EPRI handbook [17]. The explicit details of the finite element calculations and modeling procedures are discussed in a separate study [37] from the Short Cracks in Piping and Piping Welds Program [8]. Some of these new results have also been published in a recent technical paper by Brust, Rahman, and Ghadiali [45].

Specifically, the solutions to improve the F, V, and h-functions were generated for Ramberg–Osgood coefficients $n = 1, 2, 3, 5, 7, 10$ and for several crack angles (2θ) for the following three cases:

- Short through-wall cracks under bending ($\theta/\pi = 1/16, 1/8$);
- long through-wall cracks under bending ($\theta/\pi = 1/4, 1/2$); and
- short through-wall cracks under combined bending and tension ($\theta/\pi = 1/16, 1/8$).

5.1. Short through-wall cracks under pure bending

5.1.1. Finite element model and analysis matrix

Six finite element meshes were developed, one for each case listed in Table 1. A typical finite element mesh and geometric definitions are illustrated in Fig. 3. A quarter model was used by taking advantage of symmetry. Twenty-noded, isoparametric, brick elements were used with focused elements at the crack tip. Only one element through the pipe wall was used, and, as such, the tabulated results should be considered as average values through the pipe wall.

The elastic solutions were developed using the elastic properties of the pipe. A deformation theory plasticity algorithm in the ABAQUS [46] finite element code was used to generate the plastic solution. Because a through-wall-cracked pipe subjected to bending is a plane stress problem,

Table 1
Matrix of finite element calculations for short through-wall-cracked pipes under pure bending (total of 30 analyses)

Model no.	Model name	R_m/t	n[a]	θ/π	Remarks	Loading
1	CASE1A3DM	5	1,2,3,5,7,10	0.0625	5 Runs	Bending
2	CASE2A3DM	10	1,2,3,5,7,10	0.0625	5 Runs	Bending
3	CASE3A3DM	20	1,2,3,5,7,10	0.0625	5 Runs	Bending
4	CASE1B3DM	5	1,2,3,5,7,10	0.1250	5 Runs	Bending
5	CASE2B3DM	10	1,2,3,5,7,10	0.1250	5 Runs	Bending
6	CASE3B3DM	20	1,2,3,5,7,10	0.1250	5 Runs	Bending

[a] $n = 1$ is elastic.

the special (hybrid) elements in the ABAQUS library which adequately handle plastic incompressibility are not necessary. A reduced (2 × 2) Gaussian quadrature integration rule was utilized.

5.1.2. Results of analysis

Both elastic and fully plastic (deformation theory) computations were made for bending loads for each of the six cases defined in Table 1. Past studies suggest that the original GE/EPRI compilations are accurate in predicting J for large crack sizes. Hence, a comparison was made for a specific pipe case with $R_m/t = 10$, $\theta/\pi = 1/2$, and $n = 3$ to verify the accuracy of the results from these new analyses. Table 2 lists the plastic h-functions for a pipe under pure bending obtained from Ref. [17] and the present study. The comparisons for h_1 (J-integral) indicate little difference between the results of these two finite element solutions. However, the values of the h_2 (COD) and h_4-functions (load-point rotation) from Ref. [17] are 10.5 and 17.3% higher, respectively, than those predicted by the present study.

Tables 3–6 provide the solutions compiled for all of the cases listed in Table 1. Table 3 provides the elastic solution, while Tables 4–6 provide the plastic solutions for $R_m/t = 5$, 10, and 20, respectively. Note that the GE/EPRI handbook method did not provide solutions for

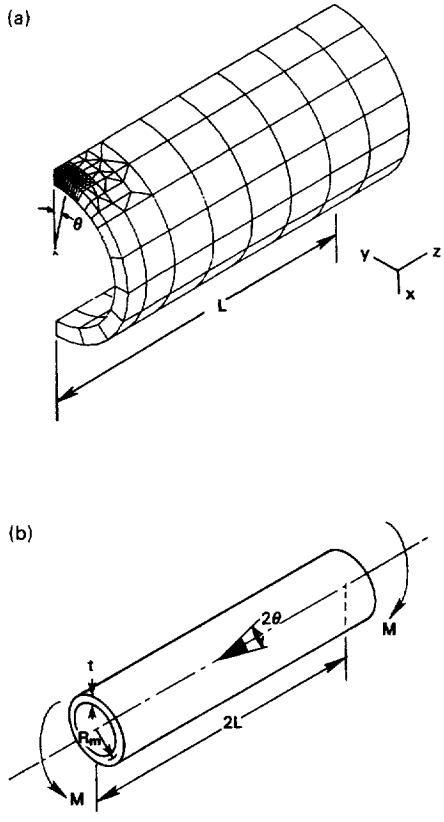

Fig. 3. Typical finite element mesh and geometric definitions (a) mesh for finite element analysis (1/4 model), (b) circumferentially cracked-pipe geometry.

Table 2
Check case $R_m/t = 10$, $\theta/\pi = 1/2$, and $n = 3$ (pure bending)

Influence functions	GE/EPRI [17]	3D-Solid ABAQUS (this paper)
h_1 (J-integral)	2.105	2.008
h_2 (Crack-opening displacement)	3.331	3.015
h_4 (Load-point rotation)	3.232	2.756

Table 3
F, V_1, V_3-functions for short through-wall-cracked pipes under pure bending (ABAQUS-3D solid element solution)[a]

Crack size	Function	$R_m/t = 5$	$R_m/t = 10$	$R_m/t = 20$
$\theta/\pi = 1/16$	F	1.022	1.049	1.097
	V_1	1.234	1.206	1.111
	V_3	0.028	0.035	0.098
$\theta/\pi = 1/8$	F	1.103	1.208	1.418
	V_1	1.388	1.480	1.482
	V_3	0.126	0.160	0.231

[a] This represents the $n = 1$ case of Table 1.

Table 4
Tabulation of h-functions for short through-wall-cracked pipes under pure bending for $R_m/t = 5$ (ABAQUS-3D solid element solution)

Crack size	Function	$n = 2$	$n = 3$	$n = 5$	$n = 7$	$n = 10$
$\theta/\pi = 1/16$	h_1	5.202	5.451	5.766	5.681	5.263
	h_2	6.686	6.896	7.003	6.715	6.087
	h_4	0.553	0.826	1.452	1.879	2.371
$\theta/\pi = 1/8$	h_1	4.575	4.484	3.976	3.372	2.464
	h_2	5.972	5.820	4.999	4.164	2.959
	h_4	0.958	1.194	1.454	1.461	1.291

Table 5
Tabulation of h-functions for short through-wall-cracked pipes under pure bending for $R_m/t = 10$ (ABAQUS-3D solid element solution)

Crack size	Function	$n = 2$	$n = 3$	$n = 5$	$n = 7$	$n = 10$
$\theta/\pi = 1/16$	h_1	5.588	6.225	6.761	6.784	6.749
	h_2	6.701	7.422	7.739	7.632	7.527
	h_4	0.745	1.156	1.802	2.220	2.826
$\theta/\pi = 1/8$	h_1	5.694	5.791	5.512	4.790	3.823
	h_2	6.619	6.654	6.319	5.329	4.221
	h_4	1.234	1.550	1.886	1.864	1.713

Table 6
Tabulation of h-functions for short through-wall-cracked pipes under pure bending for $R_m/t = 20$ (ABAQUS-3D solid element solution)

Crack size	Function	$n = 2$	$n = 3$	$n = 5$	$n = 7$	$n = 10$
$\theta/\pi = 1/16$	h_1	6.272	7.044	8.022	8.756	8.815
	h_2	7.155	7.073	8.050	8.787	8.812
	h_4	0.979	1.505	2.348	3.087	3.770
$\theta/\pi = 1/8$	h_1	8.019	8.448	8.281	7.748	6.524
	h_2	7.934	7.498	7.491	7.160	5.890
	h_4	1.730	2.216	2.738	2.963	2.728

$n = 10$ and some of the $n = 7$ cases due to numerical difficulties. No such difficulties were encountered in the present study.

5.2. Long through-wall cracks under pure bending

In order to be consistent with the functions developed for short through-wall cracks using ABAQUS 3D-solid elements, additional calculations were also performed for longer cracks. The methodology used to compute these functions is identical to that for short cracks.

5.2.1. Finite element model and analysis matrix

Six finite element meshes were developed, one for each case listed in Table 7 . The details of the mesh, solution techniques, etc, were similar to those for short cracks.

5.2.2. Results of analyses

Tables 8–11 provide the solutions compiled for all the cases listed in Table 7. Table 8 provides the elastic solution, while Tables 9–11 provide the plastic solutions for $R_m/t = 5$, 10 and 20, respectively.

Table 8
F, V_1, V_3-functions for long through-wall-cracked pipes under pure bending (ABAQUS-3D solid element solution)[a]

Crack size	Function	$R_m/t = 5$	$R_m/t = 10$	$R_m/t = 20$
$\theta/\pi = 1/4$	F	1.434	1.697	2.120
	V_1	2.008	2.379	3.079
	V_3	0.327	0.439	0.637
$\theta/\pi = 1/2$	F	2.552	3.031	3.902
	V_1	5.331	7.165	11.585
	V_3	3.792	5.228	8.567

[a] This represents the $n = 1$ case of Table 7

Table 9
Tabulation of h-functions for long through-wall-cracked pipes under pure bending for $R_m/t = 5$ (ABAQUS-3D solid element solution)

Crack size	Function	$n = 2$	$n = 3$	$n = 5$	$n = 7$	$n = 10$
$\theta/\pi = 1/4$	h_1	4.109	3.720	2.671	1.821	1.019
	h_2	5.319	4.706	3.283	2.189	1.194
	h_4	1.298	1.543	1.426	1.082	0.641
$\theta/\pi = 1/2$	h_1	1.981	1.408	0.684	0.418	0.154
	h_2	3.478	2.271	1.019	0.598	0.215
	h_4	2.927	2.034	0.936	0.543	0.196

Table 10
Tabulation of h-functions for long through-wall-cracked pipes under pure bending for $R_m/t = 10$ (ABAQUS-3D solid element solution)

Crack size	Function	$n = 2$	$n = 3$	$n = 5$	$n = 7$	$n = 10$
$\theta/\pi = 1/4$	h_1	5.952	5.169	3.475	2.895	1.689
	h_2	6.629	5.757	3.853	3.209	1.844
	h_4	1.676	1.896	1.712	1.593	1.006
$\theta/\pi = 1/2$	h_1	2.887	2.008	1.060	0.579	0.267
	h_2	4.693	3.015	1.452	0.777	0.349
	h_4	4.038	2.756	1.364	0.592	0.116

5.3. Short through-wall-cracked pipe under combined bending and tension

The GE/EPRI estimation scheme can be used to calculate fracture parameters such as J, COD, displacements, and rotations, for through-wall-cracked pipes under combined bending and tension using the following two approaches:

1. In the first approach, a nondimensional parameter λ is used to define a proportionality relationship between

Table 7
Matrix of finite element calculations for long through-wall-cracked pipes under pure bending (total of 30 analyses)[a]

Model no.	Model name	R_m/t	$n^{(a)}$	θ/π	Remarks	Loading
1	CASE4A3DM	5	1,2,3,5,7,10	0.5000	5 runs	Bending
2	CASE4B3DM	10	1,2,3,5,7,10	0.5000	5 runs	Bending
3	CASE4C3DM	20	1,2,3,5,7,10	0.5000	5 runs	Bending
4	CASE5A3DM	5	1,2,3,5,7,10	0.2500	5 runs	Bending
5	CASE5B3DM	10	1,2,3,5,7,10	0.2500	5 runs	Bending
6	CASE5C3DM	20	1,2,3,5,7,10	0.2500	5 runs	Bending

[a] $n = 1$ is the elastic case.

Table 11
Tabulation of h-functions for long through-wall-cracked pipes under pure bending for $R_m/t = 20$ (ABAQUS-3D solid element solution)

Crack size	Function	$n = 2$	$n = 3$	$n = 5$	$n = 7$	$n = 10$
$\theta/\pi = 1/4$	h_1	9.469	8.147	7.474	7.983	3.165
	h_2	8.916	7.704	5.173	2.970	1.055
	h_4	2.375	2.555	2.044	1.361	0.548
$\theta/\pi = 1/2$	h_1	5.009	3.893	2.300	2.096	1.051
	h_2	7.913	5.773	3.052	1.517	0.623
	h_4	6.611	5.023	2.727	1.379	0.572

pressure (or tension) and moment, M. The GE/EPRI plastic functions h_1, h_2, h_3, and h_4 are now also a function of λ. This approach, although theoretically rigorous, is not very convenient for pipes subjected to a fixed internal pressure and varying bending moment, which is the case in nuclear piping for boiling water reactor (BWR) and pressurized water reactor (PWR) systems. Due to the addition of one more variable (λ), the number of variables h is a function of increases from three to four. Consequently, the matrix of finite element calculations for determining these h-functions can become enormously large. Nevertheless, some limited solutions of h-functions using λ were compiled in Ref. [18].

2. In the second approach, it is proposed that the plastic h-functions be evaluated for a fixed internal pressure and increasing bending moment using procedures similar to those used for tension and bending alone (see Eq. (18)). For example, the calculated h values can be determined for an internal pressure of 15.51 MPa (2250 psi) and 7.24 MPa (1050 psi) for operating conditions at PWR and BWR plants, respectively. This is the approach undertaken by the authors to conduct new finite element calculations of the h-functions. The calculations were performed only for the PWR pressure condition i.e. for $p = 15.51$ MPa (2250 psi). No similar calculations were done for the BWR pressure condition (7.24 MPa [1050 psi]) or any other pressure. However, using the h-functions for PWR pressure should provide overpredictions of J and COD for cracked pipes at BWR pressures.

5.3.1. Finite element model and analysis matrix

Six finite element meshes were developed, one for each case listed in Table 12 . A typical finite element mesh and geometric definition are illustrated in Fig. 3. A quarter model was used to take advantage of symmetry. Twenty-noded isoparametric brick elements were used with focused elements at the crack tip. Only one element through the pipe wall was used, and, as such, the tabulated results should be considered as average values through the pipe wall.

Table 13
Tabulation of h-functions for short through-wall-cracked pipes under combined bending and tension for $R_m/t = 5$ ($p = 15.51$ MPa [2250 psi])

Crack size	Function	$n = 2$	$n = 3$	$n = 5$	$n = 7$	$n = 10$
$\theta/\pi = 1/16$	h_1	5.408	5.725	6.060	5.967	5.341
	h_2	6.851	7.115	7.232	6.979	6.153
	h_3	1.245	1.299	1.772	1.868	1.446
	h_4	2.746	1.591	2.045	2.917	3.472
$\theta/\pi = 1/8$	h_1	4.837	4.682	4.338	3.996	3.064
	h_2	6.182	5.918	5.312	4.766	3.580
	h_3	2.013	1.662	1.423	1.232	0.813
	h_4	3.279	2.020	2.285	2.608	2.133

Table 14
Tabulation of h-functions for short through-wall-cracked pipes under combined bending and tension for $R_m/t = 10$ ($p = 15.51$ MPa [2250 psi])

Crack size	Function	$n = 2$	$n = 3$	$n = 5$	$n = 7$	$n = 10$
$\theta/\pi = 1/16$	h_1	5.929	6.409	7.157	8.052	8.312
	h_2	6.973	7.460	8.108	8.923	9.009
	h_3	1.524	1.643	2.264	2.647	2.702
	h_4	2.507	1.893	3.199	6.191	9.048
$\theta/\pi = 1/8$	h_1	6.051	6.066	6.206	5.618	6.294
	h_2	6.888	6.868	6.844	6.181	6.578
	h_3	1.652	1.533	1.459	1.187	1.585
	h_4	2.624	2.089	3.055	3.036	4.495

5.3.2. Results of analysis

The plastic h-functions for pipes in Table 12 that are subjected to combined bending and tension due to an internal pressure of 15.51 MPa (2250 psi) are given in Tables 13–15 for $R_m/t = 5$, 10, and 20, respectively.

5.4. Discussions of the results

The differences between the solutions developed previously [16–18] and the present results appear to be most important for small crack sizes (e.g. when $\theta/\pi = 1/16$ and 1/8). The present solutions were developed using the three-dimensional solid elements (20-noded brick elements) and

Table 12
Matrix of finite element calculations for short through-wall-cracked pipes under combined bending and tension (total of 30 analyses)

Model no.	Model name	R_m/t	n	θ/π	Remarks	Loading
1	CASE1A3DTM	5	2,3,5,7,10	0.0625	5 Runs	Tension and bending
2	CASE2A3DTM	10	2,3,5,7,10	0.0625	5 Runs	Tension and bending
3	CASE3A3DTM	20	2,3,5,7,10	0.0625	5 Runs	Tension and bending
4	CASE1B3DTM	5	2,3,5,7,10	0.1250	5 Runs	Tension and bending
5	CASE2B3DTM	10	2,3,5,7,10	0.1250	5 Runs	Tension and bending
6	CASE3B3DTM	20	2,3,5,7,10	0.1250	5 Runs	Tension and bending

Table 15
Tabulation of h-functions for short through-wall-cracked pipes under combined bending and tension for $R_m/t = 20$ ($p = 15.51$ MPa [2250 psi])

Crack size	Function	$n = 2$	$n = 3$	$n = 5$	$n = 7$	$n = 10$
$\theta/\pi = 1/16$	h_1	6.734	7.484	10.251	13.544	15.243
	h_2	7.561	8.292	10.924	14.078	15.813
	h_3	1.210	1.369	2.479	3.696	3.870
	h_4	2.144	2.264	6.069	11.739	17.100
$\theta/\pi = 1/8$	h_1	8.621	8.917	10.846	13.282	13.836
	h_2	8.375	8.705	10.383	12.479	13.051
	h_3	1.289	1.367	1.577	2.223	2.317
	h_4	2.689	2.778	5.160	7.720	9.046

the deformation theory algorithm of ABAQUS. The solutions presented here are believed to be the more accurate of the two solutions because full three-dimensional elements were used instead of relying on shell elements. The analyses presented in Ref. [17] appear to produce results that are too stiff, and, indeed, solutions for large n were not possible as convergence problems occurred. In our analysis, no convergence problems were experienced. The problems with the short-crack solutions of Ref. [17] are discussed in much more detail in Refs [21,22].

The plots of the new F-function results and the corresponding GE/EPRI solutions are seen in Fig. 4(a) as a function of R_m/t for $\theta/\pi = a/b = 1/16$. The differences are about three percent. Fig. 4(b) shows two plots of V_1 that are related to the elastic crack-opening displacement. The values of V_1 obtained from the present work and the GE/EPRI solution show different trends as a function of R_m/t. From Fig. 4(b), the largest difference is about 20% for $R_m/t = 5$. Comparisons of h_1 (J-integral) and h_2 (crack-opening displacement) values are presented in Figs. 5 and 6, respectively. The h_1 and h_2 values differ less than 25% between the two solutions.

No comparisons were made for the h_4 functions. The original GE/EPRI h_4 functions are negative for most small-crack cases that were developed in Ref. [17] and were obviously in error.

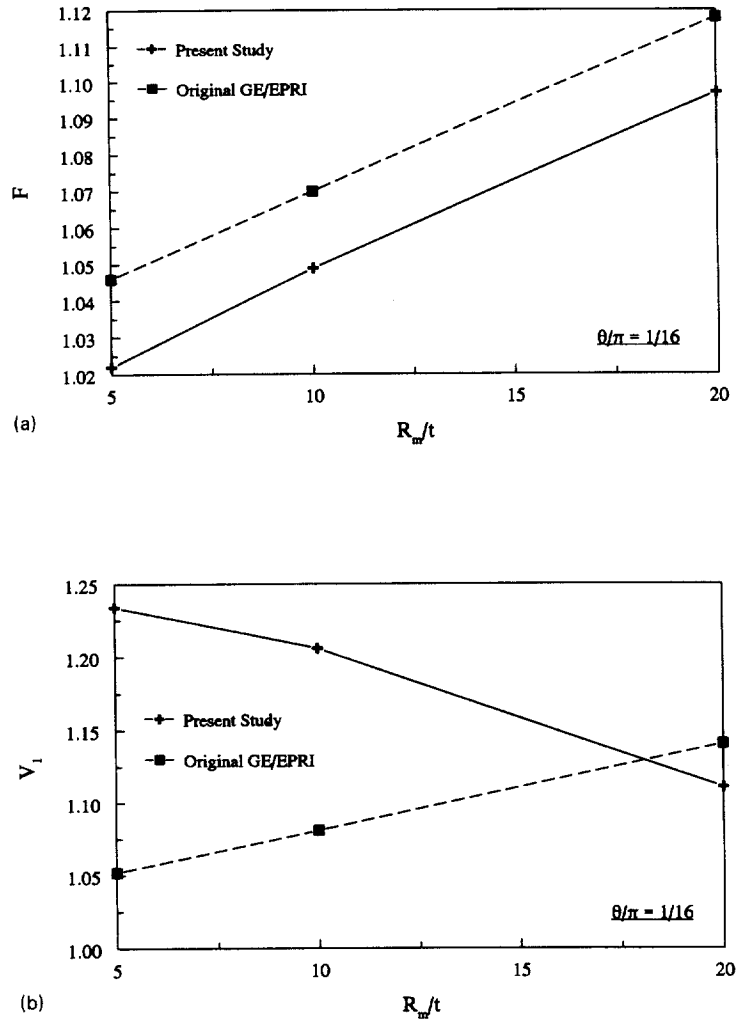

Fig. 4. Comparison of ABAQUS FEM results to past GE/EPRI solutions for elastic functions (a) F-function for $\theta/\pi = 1/16$ (F relates elastic stress intensity factor to stress), (b) V_1 function for $\theta/\pi = 1/16$ (V_1 relates elastic center-crack-opening displacement to moment).

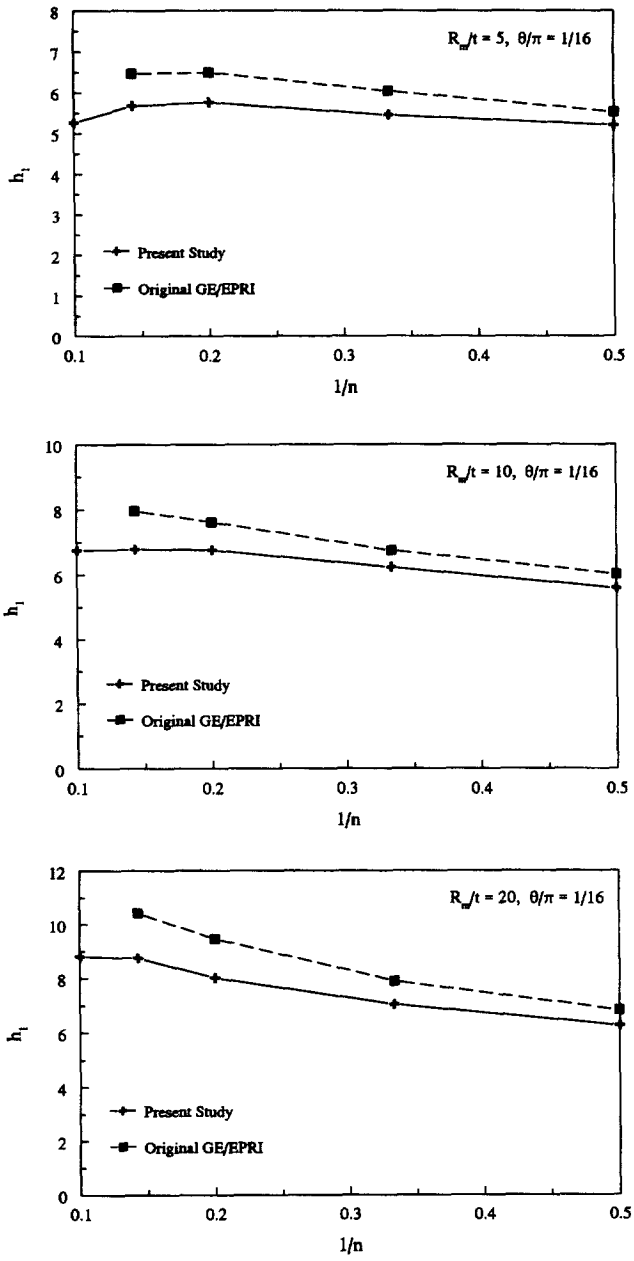

Fig. 5. Comparison of ABAQUS FEM results to past GE/EPRI solutions for h_1 fully plastic functions (h_1 relates fully plastic J to moment).

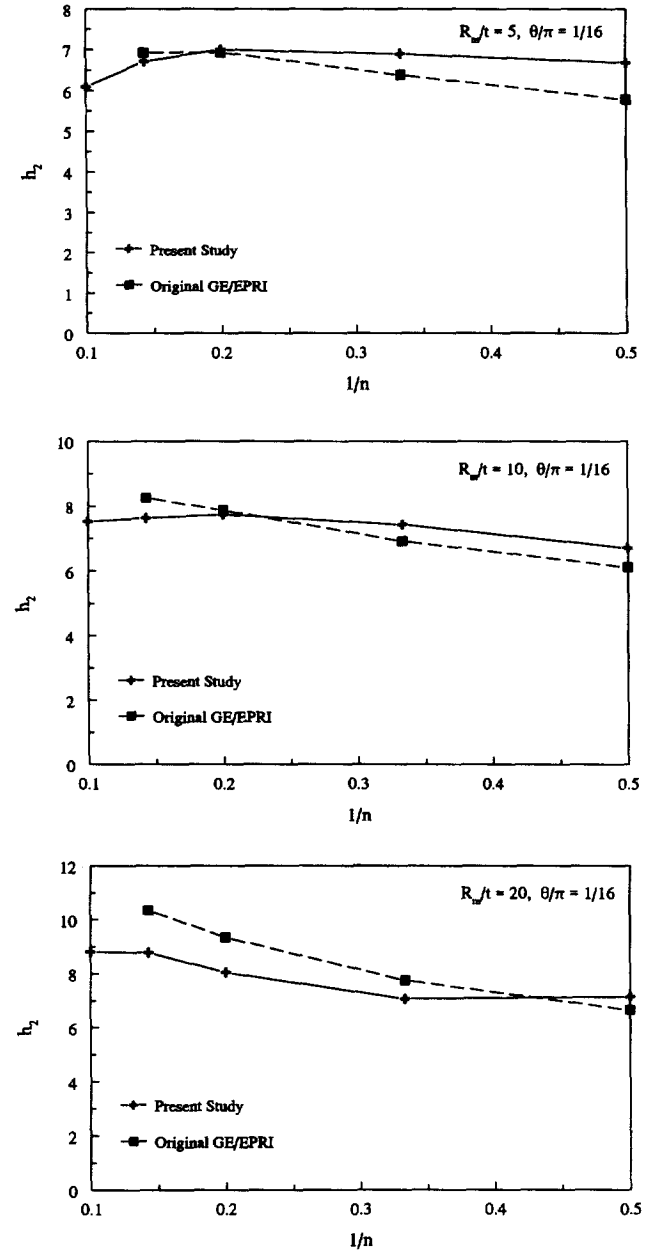

Fig. 6. Comparison of ABAQUS FEM results to past GE/EPRI solutions for h_2 fully plastic functions (h_2 relates fully plastic center-crack-opening displacement to moment).

5.5. Considerations of hoop stress in pipes due to pressure

The new GE/EPRI h-functions for combined bending and tension were calculated using two load steps. An axial tension (corresponding to internal pressure) was applied to the end of the pipe, and then the bending moment was increased. Hence, none of the influence functions computed in Ref. [17] and the present study accounts for hoop (circumferential) stress in a pipe due to the internal pressure.

In order to evaluate the effects of hoop stress in a pipe, an additional analysis was performed. In this particular analysis, the load in the first step consisted of axial tension and internal pressure applied to all inside pipe elements. The second step was identical to the previous analysis, i.e. an increasing bending load was applied until fully plastic conditions were reached.

The analysis was performed for a short crack using Model 2 in Table 12 with $R_m/t = 10$, $\theta/\pi = 0.0625$, and $n = 5$. Table 16 shows the h-functions from this analysis and the corresponding results where no internal pressure was applied (i.e. only axial tension was applied). The comparisons of results suggest that the hoop stress due to pressure increases h_1, and hence, J. The mid-thickness

Table 16
Tabulation of h-functions for through-wall-cracked pipes under combined bending and tension with and without hoop stresses due to internal pressure of 15.51 MPa (2250 psi) [$R_m/t = 10$, $\theta/\pi = 0.0625$, and $n = 5$]

Plastic Function	Load	
	Axial Tension and Bending	Hoop Stress, Axial Tension, and Bending
h_1 (J)	7.157	7.605
h_2 (COD)	8.108	8.247
h_3 (load-point axial displacement)	2.264	0.549
h_4 (rotation)	3.199	1.952

crack-opening displacement (h_2) was also increased slightly. This may be due to local crack bulging. The load-point axial displacement (h_3) and the pipe rotation (h_4) were significantly affected due to stiffening of the pipes under additional hoop stresses.

6. Summary and conclusions

A comprehensive review is performed to determine the current state-of-the art in predicting crack-opening displacements for a cracked pipe under pure bending, pure tension, and combined bending and tension loads. New and improved analytical models and their preliminary results are presented for cases where current methods are not available or inadequate. For example, a new estimation method (LBB.ENG3) was developed to predict crack-opening area of a pipe with cracks in the center of the weld. The method is based on an equivalence criterion incorporating reduced thickness analogy for simulating system compliance due to the presence of a crack in the pipe.

The GE/EPRI influence functions were computed by elastic-plastic finite-element analyses to determine the J-integral, crack-opening displacement, and other fracture parameters. The differences between the previously developed solutions (EPRI NP-3607) and the present results appear to be most important for small crack sizes (e.g. when $\theta/\pi = 1/16$ and $1/8$). The present solutions were developed using the three-dimensional solid elements (20-noded brick elements) and the deformation theory algorithm of ABAQUS. The solutions presented here are believed to be the more accurate of the two solutions because full three-dimensional elements were used instead of relying on shell elements. The influence functions in EPRI NP-3607 report appear to produce results that are too stiff, and, indeed, solutions for large n were not possible as convergence problems occurred. No convergence problems were experienced in the present work.

For pipes under combined bending and pressure, the influence functions for a specific pipe ($R_m/t = 10$, $\theta/\pi = 1/16$, and $n = 5$) were compared to determine the effects of hoop stress on a pipe. The comparisons of results suggest that the hoop stress due to pressure would increase h_1, and hence, the J-integral. The mid-thickness crack-opening displacement (h_2) was also increased slightly. This may be due to local crack bulging. The load-point displacement (h_3) and the pipe rotation (h_4) were significantly affected due to stiffening of the pipe under additional hoop stresses.

Acknowledgements

The authors would like thank Mr. Michael Mayfield and the U.S. NRC Office of Research, Electrical, Materials, and Mechanical Engineering Branch for their encouragement and support of this effort as part of the US NRC's 'Short Cracks in Piping and Piping Welds' Program, Contract No. NRC-04-90-069.

References

[1] Rahman S, Brust FW, Ghadiali N, Wilkowski G. Crack-opening-area analyses for circumferential through-wall cracks in pipes—Part II: model validations. International Journal of Pressure Vessels and Piping, 1998;75(5):375–396.

[2] Rahman S, Ghadiali N, Wilkowski G, Moberg F, Brickstad B. Crack-opening-area analyses for circumferential through-wall cracks in pipes—Part III: off-center cracks, restraint of bending, thickness transition, and weld residual stresses. International Journal of Pressure Vessels and Piping, 1998;75(5):397–415.

[3] Report to the US Nuclear Regulatory Commission Piping Review Committee, Prepared by the Pipe Break Task Group, NUREG/CR-1061, Vol. 3. Washington, DC: US Nuclear Regulatory Commission, November 1984.

[4] Published for public comment on Standard Review Plan, Section 3.6.3 Leak-Before-Break Evaluation Procedures, Federal Register, Vol. 52, No. 167, Notices, pp. 32626–32633, Friday, August 28, 1987.

[5] Rahman S, Brust F, Ghadiali N, Choi YH, Krishnaswamy P, Moberg F, Brickstad B, Wilkowski G. Refinement and evaluation of crack-opening-area analyses for circumferential through-wall cracks in pipes, NUREG/CR-6300. Washington, DC: US Nuclear Regulatory Commission, April 1995.

[6] Wilkowski GM, Ahmad J, Barnes CR, Brust F, Ghadiali N, Guerrieri D, Jones D, Kramer G, Landow M, Marschall CW, Olson, R, Papaspyropoulos V, Pasupathi V, Rosenfeld M, Scott P, Vieth P. Degraded piping program—Phase II: Summary of technical results and their significance to leak-before-break and in-service flaw acceptance criteria, March 1984–January 1989, NUREG/CR-4082, Vol. 8. Washington, DC: US Nuclear Regulatory Commission, 1989.

[7] Schmidt RA, Wilkowski GM, Mayfield ME. The international piping integrity research group (IPIRG) program: an overview. In: H. Shibata, editor, Transactions of the 11th International Conference on Structural Mechanics in Reactor Technology, Vol. G2: Fracture Mechanics and Non-Destructive Evaluation—2. Tokyo, Japan, Paper No. G23/1. August 1991:177–188.

[8] Wilkowski GM and others. Short cracks in piping and piping program. Semiannual reports by Battelle, NUREG/CR-4599, Vols. 1 to 3, Nos. 1 and 2. Washington, DC: US Nuclear Regulatory Commission, 1991–1994.

[9] Erdogan F. Fracture analysis of pipelines containing circumferential flaws. Second annual report, US Department of Transportation, Contract No. DOT-RC-82007, June 1980.

[10] Erdogan F, Delale F. Ductile fracture of pipes and cylindrical containers with a circumferential flaw. Transactions ASME, Journal of Pressure Vessel Technology, 1981;103:160–168.

[11] Sanders JL Jr. Circumferential through-cracks in cylindrical shells under tension. Journal of Applied Mechanics, 1982;49:103–107.
[12] Sanders JL Jr. Circumferential through-crack in a cylindrical shell under combined bending and tension. Journal of Applied Mechanics, 1983;50:221.
[13] Yoo SH, Pan J. Closed form displacement solutions for circumferentially cracked pipes in bending and tension. Ann Arbor, MI: University of Michigan Report No. UM-MEAM-88-06, October 1988.
[14] Tada H, Paris PC, Irwin GR. The stress analysis of cracks handbook. Hellertown: Del Research Corp., 1973.
[15] Wuthrich C. Crack opening areas in pressure vessels and pipes. Engineering Fracture Mechanics, 1983;18:5.
[16] Kumar V, German M, Shih C. An engineering approach for elastic-plastic fracture analysis. EPRI Report NP-1931. Palo Alto, CA: Electric Power Research Institute, July 1981.
[17] Kumar V, German M, Wilkening W, Andrews W, deLorenzi H, Mowbray D. Advances in elastic-plastic fracture analysis. EPRI Final Report NP-3607. Palo Alto, CA: Electric Power Research Institute, August 1984.
[18] Kishida K, Zahoor A. Crack-opening area calculations for circumferential through-wall pipe cracks. EPRI Special Report NP-5959-SR. Palo Alto, CA: Electric Power Research Institute, August 1988.
[19] Paris PC, Tada H. The application of fracture proof design methods using tearing instability theory to nuclear piping postulating circumferential through-wall cracks. NUREG/CR-3464. Washington, DC: US Nuclear Regulatory Commission, September 1983.
[20] Klecker R, Brust F, Wilkowski G. NRC leak-before-break (LBB.NRC) analysis method for circumferentially through-wall-cracked pipes under axial plus bending loads. NUREG/CR-4572, Washington, DC: US Nuclear Regulatory Commission, May 1986.
[21] Brust FW. Approximate methods for fracture analyses of through-wall cracked pipes. NUREG/CR-4853. Washington, DC: US Nuclear Regulatory Commission, February 1987.
[22] Gilles P, Brust F Approximate fracture methods for pipes. Part I: theory. Nuclear Engineering and Design, 1991;127:1–27.
[23] Gilles P, Chao KS, Brust F. Approximate fracture methods for pipes. Part II: Applications. Nuclear Engineering and Design, 1991;127:13–31.
[24] Rahman S, Brust F, Nakagaki M, Gilles P. An approximate method for estimating energy release rates of through-wall cracked pipe weldments. Fatigue, Fracture, and Risk 1991:215, San Diego, CA.
[25] Rahman S, Brust F. An estimation method for evaluating energy release rates of circumferential through-wall cracked pipe welds. Engineering Fracture Mechanics, 1992;43(3):417–430.
[26] Rahman S, Brust F. Elastic–plastic fracture of circumferential through-wall cracked pipe welds subject to bending. Journal of Pressure Vessel Technology, 1992;114(4):410–416.
[27] Rice JR. A path-independent integral and the approximate analysis of strain concentration by notches and cracks. Transactions ASME Journal of Applied Mechanics, 1968;35:376–386.
[28] Rice JR, Rosengren GF. Plane strain deformation near a crack-tip in a power-law hardening material. Journal of the Mechanics and the Physics of Solids, 1968;16:1–12.
[29] Hutchinson JW. Singular behavior at the end of a tensile crack in a hardening material. Journal of the Mechanics and the Physics of the Solids, 1968;16:13–31.
[30] Hutchinson JW. Fundamentals of the phenomenological theory of nonlinear fracture mechanics. Journal of Applied Mechanics, 1982; 49:103–107.
[31] Paris PC, Tada H, Zahoor A, Ernst H. The theory of instability of the tearing mode of elastic–plastic crack growth. ASTM STP 668, Elastic–Plastic Fracture 1979:5–36.
[32] Shih CF. *J*-Dominance under plane strain fully plastic conditions: the edge crack panel subject to combined tension and bending. International Journal of Fracture, 1985;29:73–84.
[33] Shih CF, Hutchinson JW. Combined loading of a fully plastic ligament ahead of an edge crack. Journal of Applied Mechanics 1986; (53):271.
[34] Kaiser S. An extension of tearing instability theory to multiple loading parameters. International Journal of Fracture, 1985;29:85–99.
[35] Sonnerlind H, Kaiser S. The *J*-integral for a SEN specimen under nonproportionally applied bending and tension. Engineering Fracture Mechanics, 1986;24(5):637–646.
[36] Brust FW, Gilles P. Approximate methods for fracture analysis of tubular members sunjected to combined tensile and bending loads. ASME Journal of Offshore Mechanics and Arctic Engineering, 1994;116:221–227.
[37] Brust FW, Scott P, Rahman S, Ghadiali N, Kilinski T, Francini B, Marschall CW, Miura N, Krishnaswamy P, Wilkowski GM. Assessment of short through-wall circumferential cracks in pipes-experiments and analysis. NUREG/CR-6235. Washington, DC: US Nuclear Regulatory Commission, April 1995.
[38] Shih CF. *J*-Integral estimates for strain hardening materials in anti-plane shear using fully plastic solutions. ASTM STP., 1976;590:3–22.
[39] Bucci RJ, Paris PC, Landes JD, Rice JR. *J*-Integral estimation procedures. ASTM STP, 1972;514:40–69.
[40] Rice JR, Paris PC, Merkle JG. Some further results of *J*-integral analysis and estimates. ASTM STP, 1973;536:231–245.
[41] Irwin GR. Plastic zone near a crack and fracture toughness. In: Proceedings of Seventh Sagamore Ordnance Materials Conference, Syracuse, Syracuse University, 1960:IV-63–IV-78.
[42] Dugdale DS. Yielding of steel sheets containing slits. Journal of Mechanics and Physics of Solids, 1960;8:100–108.
[43] Paul D, Ahmad J, Scott P, Flanigan L, Wilkowski G. Evaluation and refinement of leak-rate estimation models. NUREG/CR-5128, Rev. 1. Washington, DC: US Nuclear Regulatory Commission, June 1994.
[44] Smith E. The opening of through-wall cracks in BWR coolant lines due to the application of severe overloads. NUREG/CP-0051. Washington, DC: US Nuclear Regulatory Commission, August 1984.
[45] Brust F, Rahman S, Ghadiali N. Elastic-plastic analysis of small cracks in tubes. Journal of Offshore Mechanics and Arctic Engineering, 1995;117(1):57–62. also published in the Proceedings of the 11th International Conference on Offshore Mechanics and Arctic Engineering, Calgary, Alberta, Canada, June 1992.
[46] ABAQUS, user's guide and theoretical manual. Version 5.3. Pawtucket, RI: Hibbitt, Karlsson, and Sorensen, 1993.